AIMS Biophysics

AIMS Biophysics, 11(2): 166–189.
DOI: 10.3934/biophy.2024011
Received: 02 February 2024
Revised: 07 May 2024
Accepted: 14 May 2024
Published: 23 May 2024

http://www.aimspress.com/journal/biophysics

Research article

The role of electric charge in SARS-CoV-2 and other viral infections

Piotr H. Pawłowski[1,*] and Piotr Zielenkiewicz[2]

[1] Institute of Biochemistry and Biophysics, Polish Academy of Sciences, Warszawa, Poland
[2] Institute of Biochemistry and Biophysics, Polish Academy of Sciences, Warszawa, Poland

*** Correspondence:** Email: piotrp@ibb.waw.pl; Tel: +48226597072.

Abstract: This study analyzed the role of electric charge in human viral infections. Examples of severe acute respiratory syndrome coronavirus 2 (SARS-CoV-2), dengue, Ebola, influenza A, and respiratory syncytial virus (RSV) are presented. Charge distribution in SARS-CoV-2 and electrostatic interactions of SARS-CoV-2 with its receptor, angiotensin-converting enzyme 2 (ACE2), were evaluated, and the mean time required for respired SARS-CoV-2 virus attachment was evaluated. The virus–cell attachment modality of all of the above viruses was calculated. The impact of electric charge on other viral-related processes, such as replication of virion material, release, and immune response, was also discussed. Special charge conditions in virus treatments were also indicated.

Keywords: coronavirus; COVID-19; SARS-CoV-2; Delta; spike protein S; amino acids; dengue; Ebola; influenza A; RSV; electric charge

1. Introduction

Viral infections are any illness from a submicroscopic germ that uses host cells to reproduce. Widely known viruses are SARS, SARS-CoV-2, Ebola, influenza, Zika, yellow fever, human immunodeficiency virus (HIV), human papillomavirus (HPV), viral gastroenteritis, Varicella, and viral hepatitis [1]. Most commonly, viral infections involve the nose, throat, and upper airways or systems such as the nervous, gastrointestinal, and reproductive systems. During infection, many extra- and intracellular processes take place that involve virion material, such as the coat and envelope, and biologically important molecules of the host organism.

Macromolecules essential to life, such as proteins, nucleic acids, lipids, and carbohydrates, are

often electrically charged under physiological conditions. Specifically, macromolecule charge, reported as the statistical mean, depends on the ability of a macromolecule to gain or lose protons (H+). For example, at natural pH (7.4), lysine, arginine, and 10% of histidine residues carry a positive net charge [2]. In contrast, aspartic acid and glutamic acid residues are negatively charged. At the same pH, phosphate groups of the deprotonated deoxyribonucleic acid (DNA) and ribonucleic acid (RNA) backbone make nucleic acids highly negatively charged [3]. Moreover, pathogens have approximately 5−30% more cell membrane phospholipids (phosphatidylserine and phosphatidylglycerol) than human or plant cells. They localize mainly to the cytoplasm side of the plasma membrane leaflet and carry a hydrophilic head with a negatively charged phosphate group [4,5]. Additionally, the outer plasma membrane leaflet, covered with anionic oligosaccharides (heparan sulfate), forms the glycocalyx layer with its characteristic negative charge [6]. Thus, many structural charges in a cell are balanced via electrostatic interactions established by nearby counterion screening between molecules [7].

Many viruses have an isoelectric point (IEP) in the range of 1.9 to 8.4, with most between 3.5 and 7 [8]. For example, influenza A virus H1N1 has $4 < IEP < 4.5$ [9]. Thus, human viruses can be expected to be, in general, negatively charged under physiological conditions (pH = 7.4). More investigations regarding the virus's electric charge status have been presented in the comprehensive reviews of Luisetto [10] and Cavezzi [11]. They cite reports highlighting electrostatic interactions enhancing the spike protein's bond to host cells.

The spike protein (S) of SARS-CoV-2 plays a key role in the receptor recognition and cell membrane fusion process. It is composed of two subunits, S1 and S2. The S1 subunit contains a receptor-binding domain (RBD) that recognizes and binds to the host receptor angiotensin-converting enzyme 2 (ACE2), first opened by the accompanying cofactor, heparan sulfate. This binding exposes the cleavage sites, S1/S2, at the S1-S2 junction and, S2, upstream of the fusion peptide, to cellular proteases. Cleavage of the spike led the S1 subunit to dissociate and transform the conformation of the S2 subunit, which exposes the hydrophobic region (HR1), allowing the fusion peptide (FP) to insert into the host cells. Then forming a six-helical bundle via the two-heptad repeat domain with the hydrophobic region (HR2) brings the virus and host cell closer. This completes the fusion and begins the virus internalization.

Going back to the reports, Northwestern University reported, "Using nanometer-level simulations, researchers have discovered a positively + charged site (known as the polybasic cleavage site) located 10 nanometers from the actual binding site on the spike protein. The positively charged site allows strong bonding between the virus protein and the negatively charged human-cell receptors" [12].

Leung and Sun reported, "By using the multilayer/multimodule approach using either small-diameter nano-fibers with small basis weight in the modules, or large-diameter nano-fibers with large basis weight in the modules, high-performance charged nanofiber filters have been developed that achieve over 90% capture of airborne COVID-19 simulated by the 100-nm sodium chloride aerosols." In addition, "If the coronavirus is negatively charged, the positively charged PVDF (polyvinylidene fluoride—from the author) nanofiber filter will provide even higher capture efficiency as well by Coulomb attraction" [13].

According to Giron [14], Luisetto wrote, "Recent experimental evidence has shown the ability of the SARS-CoV-2 spike protein to bind SA (sialic acid —from the author) molecules embedded in the membrane glycoproteins. In view of its negative charge, SA has a role in the determination of cell

membrane electrical charge and the consequent binding to the electrically positive charged spike protein S1"**.**

The subject of the present manuscript is the role of the electric charge in various human viral infections. Considered examples of viruses are SARS-CoV-2, dengue, Ebola, influenza A, and RSV. Molecular regions of interest comprise structural elements of the virus and cell surface as well as nonstructural enzymatic proteins involved in the process of infection.

The main objective of this study is to identify the molecular regions of the host and virus, which have an imbalanced overall electric charge, which may be important in facilitating virus attachment and entry, controlling viral replication and release, strengthening the immune response, and therapeutic targeting. The above can be an intermediate goal on the road toward finding an effective virus treatment. Recently, many interesting works have appeared related to this theme, especially on characteristics of new variants of SARS-CoV-2, i.e., Alpha, Beta, Gamma, Delta, and Omicron [15,16]; its categorization [17] on coronavirus disease 2019 (COVID-19) management, diagnosis, treatment, and vaccination [18–21]; and on the overall view of the pandemic situation [22]. Biophysical modeling showed that external electric fields of easily achievable and moderate strengths can dramatically destabilize the S protein, inducing long-lasting structural damage almost preventing binding to the ACE2 receptor [23].

First, the charge distribution in SARS-CoV-2 and electrostatic interactions of SARS-CoV-2 with the receptor ACE2 were evaluated. This made it possible to show the dominant importance of local spatial distribution, as opposed to the overall quantity of charge, and to estimate the mean time required for SARS-CoV-2 virus attachment. As a consequence of the assumed dominant impact of a local electric charge, an estimation of the charge of chosen immunologically important single proteins allowed the analysis of the virus-cell attachment modality of all viruses studied. The impact of electric charge on other viral-related processes, such as replication of virion material, release, and immune response, is also discussed. Special charge conditions in virus treatments are indicated. It was shown that they may have an impact on SARS-CoV-2 treatment prognoses. Some papers regarding the role and mutations of the electric charge in SARS-CoV-2 were already published. These publications analyzed changes in the total charge on the spike protein of SARS-CoV-2 in emerging lineages [24], electrostatic interaction between SARS-CoV-2 virus and charged electret fiber [25], and surface charge changes in spike RBD mutations of SARS-CoV-2 altering evasiveness [26]. The innovative aspect of the article presented below consists of estimating physical parameters (charges, energies) regarding the non-structural catalytic role of a charge and includes considerations for other viruses.

2. Materials and methods

In the analysis of the spatial distribution of electric charge in "wild-type" SARS-CoV-2, a simple model of the organization of virion components was proposed (Figure 1) using details from a comprehensive report [27]. Basic protein data files were taken from The Research Collaboratory for Structural Bioinformatics Protein Data Bank (RCSB PDB) [28] in FASTA format and from The National Center for Biotechnology Information (NCBI) [29] in GenBank format. The charge per protein was calculated arithmetically by subtracting the number of negatively charged amino acids from the number of positively charged ones in the protein sequence at pH = 7.4. The assumed charge was for aspartic acid (Asp) and glutamic acid (Glu) -1 [e], for histidine (His) 0 [e], for lysine (Lys)

and arginine (Arg) +1 [e]. The charge of the proteins for other viruses was calculated in the same manner. Each dataset used is referenced separately in the following text.

The electric field intensity E and the electrostatic energy U were estimated using a screened Coulomb interaction formula in the Debye–Hückel (or Yukawa) form [30]:

$$E = QExp(-r/L_D)/(4\pi\varepsilon_0\varepsilon r^2) \quad \text{(Eq 1)}$$

$$U = Q_1Q_2Exp(-r/L_D)/(4\pi\varepsilon_0\varepsilon r) \quad \text{(Eq 2)}$$

where: Q is a charge, Q_1 and Q_2 are interacting charges, $Exp()$ is the exponential function, r is the interaction distance, L_D is the Debye screening length, ε_0 is the dielectric permittivity of vacuum, and ε is the relative dielectric constant of the medium.

Epidemiologic data were extracted from Public Health England reports [31,32].

Multiple alignment of sequences of the receptor binding motif (RBM) in SARS-CoV-2 variants was performed with the help of CLUSTAL O (1.2.4) (https://www.ebi.ac.uk/jdispatcher/msa/clustalo). Data for variants were taken from the Stanford University Coronavirus Antiviral & Resistance Database (https://covdb.stanford.edu/variants/alpha/).

For a charge analysis at different pH values, Protein Calculator v3.4 was applied (https://protcalc.sourceforge.net) to take into account the exact amino acid charge gained due to the dissociation processes (valid for isolated residues). The charges for other molecules were taken from the literature and referenced according to the order in which they appear in the text.

3. Results

Note: Data in Table 1, Table 2, Figure 6a, and Figure 6b are the estimates, statistical averages, or real data. Data in Figure 1, Figure 2, Figure 3, Figure 4, Figure 5, Figure 7, and Figure 8 are model or theoretical predictions.

3.1. Analysis of the charge distribution in SARS-CoV-2

The charge on a virus is unevenly distributed. In the case of SARS-CoV-2 ("wild-type"), looking from the inside to the outside, we can see that the charge distribution is related to the main virus components (Figure 1), i.e., the RNA, nucleocapsid proteins (N), membrane phospholipids (P), membrane proteins (E and M), and surface spike proteins (S), with the characteristic receptor-binding domain (RBD) and stalk (St), mostly covering the main functional subunits of the spike protein, S1 and S2. This perspective allowed us to calculate the approximate localized charge (Table 1).

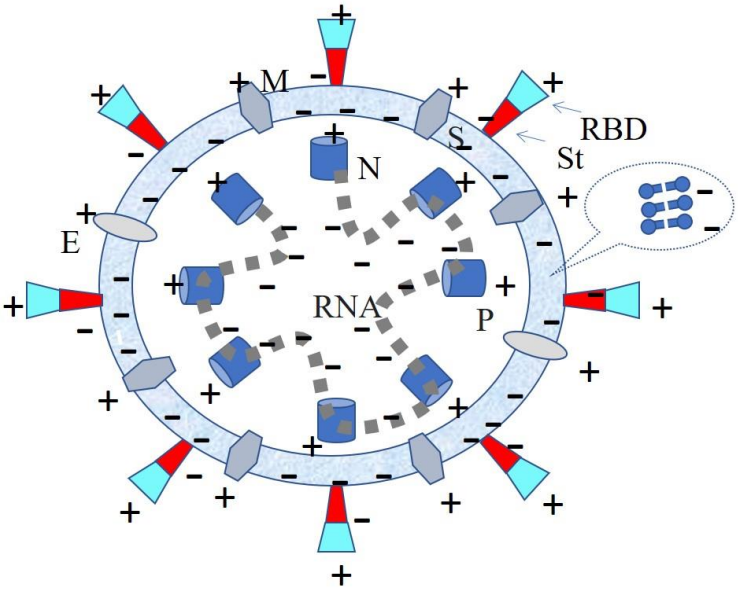

Figure 1. The main SARS-CoV-2 components are RNA, nucleocapsid proteins (N), membrane phospholipids (P), membrane proteins (M and E), and surface spike proteins (S), containing the stalk (St) and receptor-binding domain (RBD). This illustrative model was inspired by the graphic presented in the comprehensive review of the state of knowledge [27]. Spherical symmetry is a reasonable approximation for this work. The RNA shape is an artistic vision neglecting its secondary and tertiary structure. Theoretically, it may contribute to the electric multipolar potential outside the virus, but at a rough estimation, it may be neglected due to fast vanishing with the distance and a screening effect.

The data shown in Table 1 were used to estimate the total charge of SARS-CoV-2 ("wild-type"), which was found to be equal to −4650 [e]. As mentioned above, a negative total charge is typical for viruses. The negatively charged regions of SARS-CoV-2 predominate in the envelope due to charged phospholipids and on the external surface due to the negative net charge of the S protein stalk. The separation of the negative and positive net charges in protein S between the stalk and RBD is in agreement with the value of the estimated [33] or determined isoelectric point [34,35].

Next, the input to the electric field intensity E from the charge in the virus region of interest, i.e., RNA and nucleocapsid, envelope, external surface, total binding area, and the total virus (Table 1) were estimated according to Eq 1, placing the charge of a given region in the center of the virion sphere (Figure 2).

Table 1. Estimated electric charge distribution on SARS-CoV-2 ("wild-type") particles.

Molecule	Number	Charge/molecule [e]	Ref.	Charge in the region of interest
RNA nucleotide	29900 [a]	-1[b]	[3,27]	RNA and nucleocapsid +6100
Nucleocapsid protein N	1500 [a]	+24 [c]	[27]	
Phospholipid	17,000 [d,e,f]	-1 [g]	[4,5,33,34]	Envelope -8950
Protein E	25 [a]	+2 [c]	[27]	
Protein M	1000 [a]	+8 [c]	[27]	
Protein S (stalk)	150 [a]	-19 [h,c]	[27]	External surface -2850
Protein S 0(RBD)	150 [a]	+7 [h,c]	[27]	Total binding area +1050
SARS-CoV-2 virion	1			Total virus -4650

Note: + a. [27], b. [3], c. GenBank: MN908947.3 Severe acute respiratory syndrome coronavirus 2 isolate Wuhan-Hu-1, complete genome, d. [5], e. [33], f. [34], g. [4], h. RCSB PDB: > 6M0J_2|Chain B [auth E]|Spike protein S1|Severe acute respiratory syndrome coronavirus 2 (2697049).

The charge per protein was calculated by subtracting the number of negatively charged amino acids from the number of positively charged amino acids in the protein sequence at pH = 7.4 (charge of His = 0). The charge of the stalk refers to the charge of protein S that does not include the RBD. The charge for each region was calculated by multiplying the number of its molecules by the overall single-molecule charge for each molecule type and adding the results for all molecule types in the region. The charge estimation for 20% of charged phospholipids [5] covering the viral surface, which is equivalent to a sphere with a 45-nm radius [33] and in which the area per lipid is 0.6 nm^2 [34], is shown. An electric charge of −1 [e] for the phospholipids (typical for phosphatidic acid and phosphatidylserine [4]) was assumed. The number of RNA nucleotides and proteins was obtained from a comprehensive review [27]. The RCSB PDB data file in FASTA format and NCBI data file in GenBank format were used to localize amino acids and obtain the protein charge.

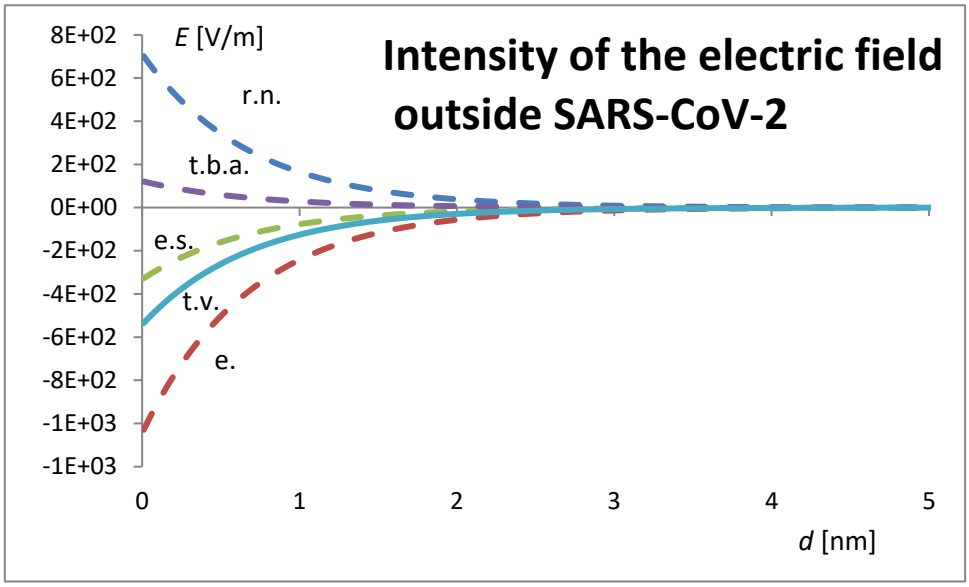

Figure 2. Intensity of the electric field outside SARS-CoV-2. Modified Eq 1 was applied for a charge Q of a given region (Table 1) placed in the center of a virion sphere. $E = QExp(-(d+s)/L_D)/(4\pi\varepsilon_0\varepsilon(d+R)^2)$, where variable d is the distance between the ACE2 central point and the nearest point of the virus; s = 10 nm is the assumed thickness of the additional screening ion penetration layer between spikes; L_D = 0.7 nm is the Debye screening length; ε_0 = 8.854E-12 F/m is the dielectric permittivity of a vacuum; ε = 80 is the relative permittivity of water; and R = 60 nm is the external radius of the virus (with the spikes included). The variable d is the distance between the ACE2 central point and the nearest point of the virus, $d = R-r$, where R = 60 nm is the assumed virus external radius and r is the ACE2 distance from the virus center. Abbreviation meanings: r.n. = RNA and nucleocapsid, e = envelope, e.s. = external surface, t.b.a. = total binding area, and t.v. = the total virus.

3.2. Analysis of the electrostatic interaction between SARS-CoV-2 and ACE2

As previously reported [36], within a single-nanometer distance, the negatively charged spike protein S is attracted to the negatively charged receptor ACE2 with an energy that exceeds that of thermal fluctuations (Figure 3). This is due to the closer proximity of ACE2 to the positively charged RBD than to the negative charge of the stalk. Therefore, the repulsion of the latter is overwhelmed by the attraction of the former.

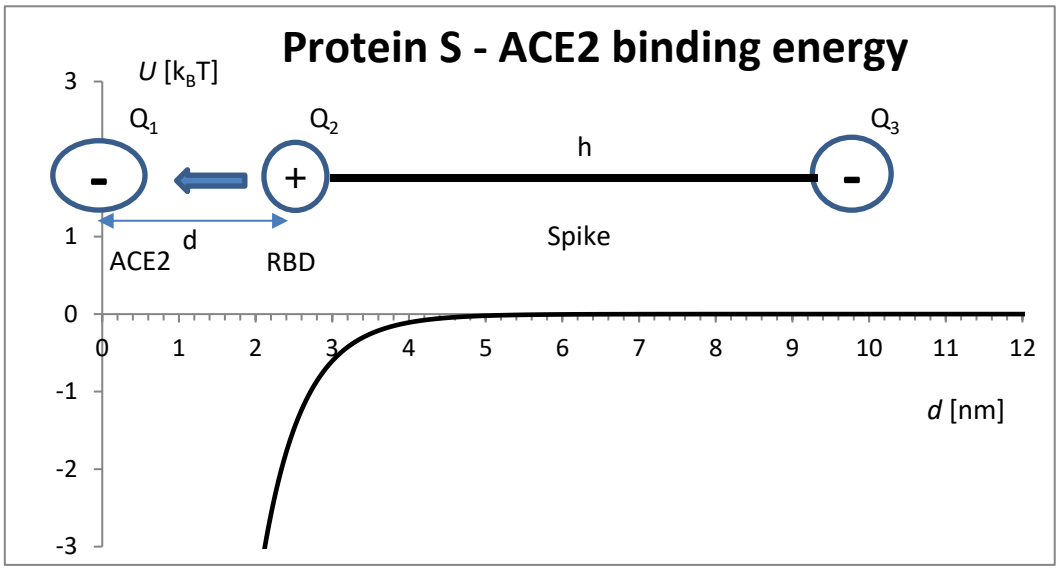

Figure 3. The estimated electrostatic binding energy between protein S ("wild-type") and the receptor ACE2 (data taken from [36]). Protein S was modeled as a nonideal dipole (with an imbalance between the charge of the RBD and that of the stalk), and ACE2 was modeled as a charged point. All charges were considered to be screened in an electrolytic environment. The potential electrostatic screening energy, U, was estimated as a function of the distance, d, between the receptor charge and the nearest protein point, according to the screened Coulomb energy formula (using Eq 2): $U = Q_1Q_2Exp(-d/L_D)/(4\pi\varepsilon_0\varepsilon d) + Q_1Q_3Exp(-(d+h)/L_D)/(4\pi\varepsilon_0\varepsilon(d+h)))$, where $Q_1 = -28$ [e] is the ACE2 net charge; $Q_2 = +7$ [e], which is the RBD net charge; the variable d is the distance between the central point in ACE2 and the nearest point on protein S; $L_D = 0.7$ nm, which is the Debye screening length; $\varepsilon_0 = 8.854E\text{-}12$ F/m, which is the dielectric permittivity of a vacuum; $\varepsilon = 80$, which is the relative permittivity of water; $Q_3 = -19$ [e], which is the stem net charge; and $h = 7.5$ nm is the dipole length, approximated by three-fourths of the spike length (10 nm) [27]. Illustrative symbols of spike protein S and ACE2 charges are not drawn to scale.

It is reasonable to wonder whether the large negative remaining charge of SARS-CoV-2 (the overall charge of the virus minus the charge of the spike) may prevent protein S from binding to ACE2. To evaluate this possibility, the energy of the electrostatic repulsion between the virus, modeled as a homogenous sphere carrying the remaining charge, and the point charge representing the net charge of the receptor ACE2, which were both screened in a natural ionic extracellular environment, was estimated (Figure 4).

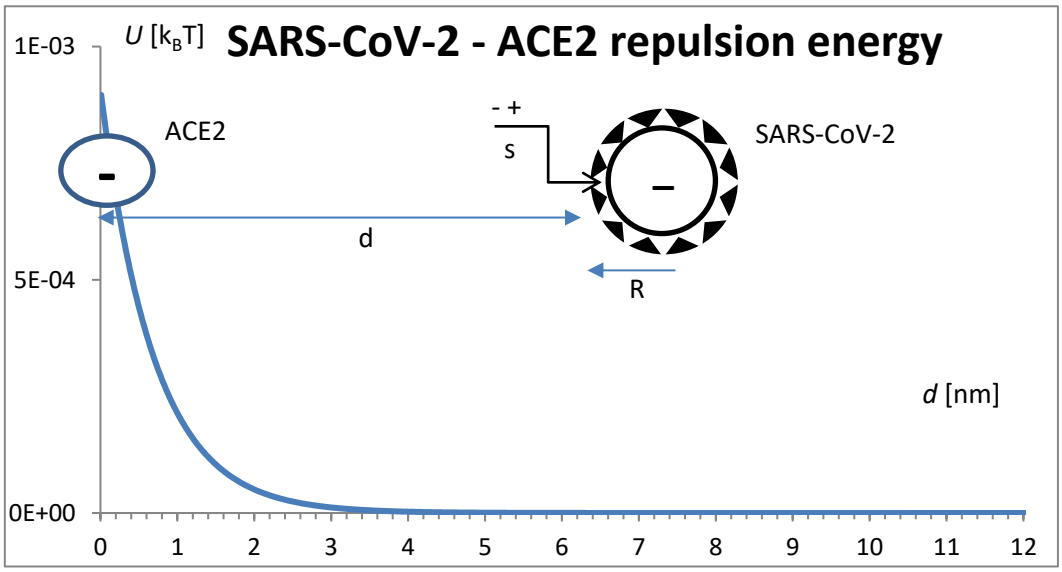

Figure 4. The estimated electrostatic repulsion energy between SARS-CoV-2 and the receptor ACE2. SARS-CoV-2 ("wild-type") was modeled as a homogenous sphere carrying an overall charge, and ACE2 was modeled as a charged point. The Gauss macroscopic field approximation was applied, and all charges were considered to be screened in an electrolytic environment. The electrostatic energy U was calculated (using Eq. 2) with the formula $U = Q_1Q_2Exp(-(d+s)/L_D)/(4\pi\varepsilon_0\varepsilon(d+R))$, where $Q_1 = -28$ [e], which is the ACE2 net charge; $Q_2 = -4638$ [e], which is the virus remaining charge (overall virus charge - spike charge); variable d is the distance between the ACE2 central point and the nearest point of the virus; s = 10 nm is the assumed thickness of the additional screening ion penetration layer between spikes; L_D = 0.7 nm, which is the Debye screening length; ε_0 = 8.854E-12 F/m, which is the dielectric permittivity of a vacuum; ε = 80, which is the relative permittivity of water; and R = 60 nm, which is the external radius of the virus (with the spikes included). Illustrative symbols of SARS-CoV-2 and ACE2 are not drawn to scale.

The results presented in Figure 3 and Figure 4 show that the spike protein is attracted to receptor ACE2 with an energy much higher than the energy of the repulsion of the remaining charge. The sum of the electrostatic energy of attraction and repulsion is shown in Figure 5. It is negative at all values of the virus receptor distance d.

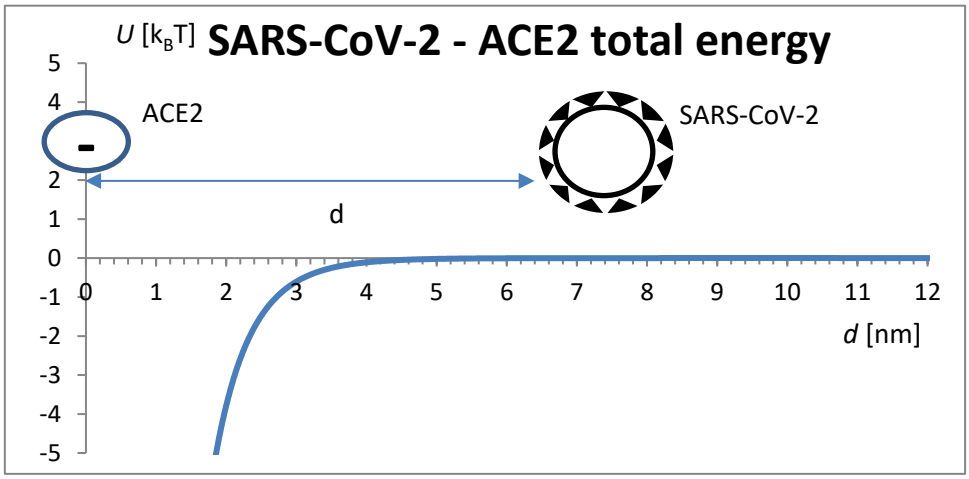

Figure 5. The sum of attraction and repulsion electrostatic energies. Variable *d* is the distance between the ACE2 central point and the nearest point of the virus. The data are based on those presented in Figure 3 and Figure 4. Illustrative symbols of SARS-CoV-2 and ACE2 are not drawn to scale.

It is reasonable to assume that the resultant electrostatic attraction is an important feature leveraged by SARS-CoV-2 to efficiently infect a host cell. The importance of this charge property is reinforced by the other positively charged residues in the crucial spike glycoprotein regions (the RBD and S1/S2 regions) in successive SARS-CoV-2 variants (Sept 2020 to Nov 2021), which have been reported in many papers [36−39].

3.3. Estimation of the mean time required for SARS-CoV-2 virus attachment

A droplet from a single cough or sneeze expelled from an infected person may contain as many as 200,000,000 virus particles [40]. This means that in a 100 m^3 area, the concentration of virus particles may reach 2,000,000 virions/m^{-3}. A healthy person entering this room within a short time (approximately one minute) after the droplet was expelled may inhale approximately n_V = 9000 viruses in each breath into the lungs, which have a 4.5–l capacity.

From the results shown in Figure 5, one can see that the energy of electrical attraction falls to −3 kT at a distance d_a equal to or less than 2.12 nm. This means that the active area (S_a) of one virus particle surface carrying 150 spike proteins (n_s) is 2100 nm^2 ($n_s\pi d_a^2$). The external spherical surface (S_t) of a virus with a radius (R) = 60 nm is 45,000 nm^2. Thus, the active area covers a proportion of k_s = 0.05 (S_a/S_t) of the total virus area.

Assuming that there are 1000 receptor ACE2 molecules [41] per spherical lung epithelial cell with a radius of 5 microns, we obtain n_r = 3 receptor ACE2 molecules per square micron of a cell surface. The active area of the cell surface (k_A) can be estimated at 0.00004 ($n_r\pi d_a^2/1{,}000{,}000$).

These results lead to an estimated probability (p) of 0.000002 (k_sk_A) that an RBD of a single virus reaches the lung surface and encounters a receptor of ACE2. Taking 10 breaths (b) within a minute, a healthy person is subjected to the action of N = 90,000 viral particles per minute (bn_V) with the probability of a single infection p. Thus, the total probability of viral-to-cell attachment during one minute of exposure to a virus-carrying droplet is p_1 = 0.2 min^{-1} (Np). Finally, the mean time required

for one virus to attach to a cell is 5 min (not considering 1 min to account for the initial replacement of air in the lungs).

3.4. An impact of the positive charge of the spike protein of SARS-CoV-2 on treatment prognosis

To analyze the possible impact of the change in spike protein charge on SARS-CoV-2 treatment prognosis, the reports of Public Health England in June and September 2021 [31,32] were considered (Figure 6a). Next, to help in the basic understanding of the mutation sites among viral proteins, multiple alignment of sequences of the receptor binding motif (RBM) in SARS-CoV-2 variants was performed indicating mutated amino acids, and confirming the increase of local positive electric charge (Figure 6b). Detailed results are presented in the Discussion.

3.5. The analysis of the overall charges of RBD and ACE2 as a function of the pH of the environment

In the context of a possible prohibition of SARS-CoV-2, the analyses of the dependence of interacting charges of RBD and ACE2 (Figure 7), and the value sign of the product of the charges (QRBD x QACE2) promoting virus-cell attachment (Figure 8) on the pH value were performed by numeric calculations. More results are presented in the Discussion.

3.6. Analysis of the cell attachment modality of other viruses

It is highly probable that other viruses also follow the aforementioned electrostatic attraction modality. Table 2 shows, as a result, collected examples of the charge of the virus-binding domain, and the host receptor of selected human viruses. The data seem to support the aforementioned hypothesis. All corresponding charges carry the opposite signs, indicating potential virus–host attractions. According to Coulomb's law [42], a negative value for the product of the charges (the charge of the binding domain x the charge of the receptor) may be considered to be an indication of the attraction strength of a virus-host cell pair at an arbitrary fixed distance. Considering this calculation, the intensive attachment of SARS-CoV-2 to a host cell is due to the exceptionally large negative receptor charge. The attraction of Ebola and its host receptor is characterized by the opposite charge distribution. Notably, similar to SARS-CoV-2, influenza A has shown an increasing binding-domain charge during its evolution [43].

Table 2. The charges of a virus binding domain and cognate host receptor.

Virus	Binding domain	Charge [e]	Host receptor	Charge [e]	Ref.
SARS-CoV-2	RBD	+7 [a]	ACE2	-28 [b]	[44]
Ebola	PS	-1[c]	TIM-1	+1[d]	[45]
Dengue	Type-3 envelope protein domain III	+1 [e]	DC-SIGN	-6 [f]	[46]
Influenza A	Hemagglutinin HA1 SUBUNIT	+6 [g]	SA	-1 [h]	[47]
RSV	RSV-G glycoprotein	+6[i]	CX3CR1	-5 [j]	[48]

Note: + a. RCSB PDB: > 6M0J_2|Chain B[auth E]|Spike protein S1|Severe acute respiratory syndrome coronavirus 2 (2697049), b. RCSB PDB: > 6M0J_1|Chain A|Angiotensin-converting enzyme 2|*Homo sapiens* (9606), c. [46], d. RCSB PDB: > 2OR8_1|Chains A, B|Hepatitis A virus cellular receptor 1 homolog|Mus musculus (10090), e. [43], f. RCSB PDB: > 6GHV_1|Chains A, B, C, D, E, F|CD209 antigen|*Homo sapiens* (9606), g. RCSB PDB: > 3LZG_1|Chains A, C, E, G, I, K|Hemagglutinin, HA1 SUBUNIT|Influenza A virus (641501), h. [47], i. RCSB PDB: > 6BLH_3|Chain C[auth G]|Major surface glycoprotein G|Human respiratory syncytial virus A (strain rsb6256) (11256), j. RCSB PDB: > 7XBW_4|Chain D[auth R]|CX3C chemokine receptor 1|*Homo sapiens* (9606). The protein charge was calculated similarly to that presented in Table 1. The required data files in FASTA format were obtained from the RCSB PDB. Phosphatidylserine (PS) and sialic acid (SA) charges [49,50] were assumed to be −1 [e].

4. Discussion

Viruses have evolved different strategies to enter the cell, but all of them, during the random diffusion, find and bind to their primary or secondary receptor(s) on the cell surface. Due to the universal electrostatic (Coulombic) attraction, the difference in the electric charge sign of the areas (the negative value sign of the charges product), of approaching virus and cell, can directly speed up this process.

In the aforementioned analysis, the role of electric charge in virus-cell attachment was described. The proposed model (3.1) of viral charge distribution (Figure 1) in a simple mesoscopic manner describes the architecture of the virion neglecting local microscopic inhomogeneities and RNA particle shape. Data in Table 1 show the largest input of the envelope charge to the total negative charge of the virus. One may mistakenly expect effective repulsion between negative virus and negative ACE2. The estimated input of the charge of the different virus areas to the intensity of the electric field outside the virus (Figure 2) shows all participations and the total value vanishing over the distances of 2 nm from the virus's extreme extending point (spike). The results (3.2) of mathematical modeling (Figure 3–5) show that the spatial (dipole-like) distribution of a charge in the spike protein S may be more important than the overall negative virus charge, which is screened by the counter ions, and finally, the dipole attraction to the host receptor prevails. What is more, the operating range of electrostatic attraction (~2 nm, Figure 5) may exceed the range of the longest hydrogen or van der Waals bonding (~0.3–0.5 nm). The proposed simple electrostatic quasi dipole-point model with Debye screening seems to be satisfactory at this point of investigation. It must be noted that molecular dynamics simulation [51] confirms the critical role of charge. On the other hand, it describes mainly the last phase of the RBD-ACE2 approach and requires many repetitions to formulate general conclusions.

The estimated mean time (3.3) required for the first SARS-CoV-2 virus-host cell attachment in an infectious environment was found to be equal to 5 min, a rate that refers only to the initial process; the process certainly accelerates as additional receptor ACE2 molecules encounter the virus. The basic idea underlying the role of electric charge in viral infection was introduced in a previous paper [52], but in addition to its role in viral attachment and fusion with a cell, when the electrical and mechanical properties of interacting structures may be crucial, electric charge may also play an important role during viral replication and release, and the host immune response. Moreover, dipoles or higher-level electric monopoles may be key structures in the catalytic centers of viral enzymes

during infection. For example, the nonstructural protein Nsp16, which is very important for protecting against SARS-CoV-2 replication, carries a mosaic charge motif +-+-, i.e., a catalytic tetrad consisting of Lys46, Asp130, Lys170, and Glu203, in its catalytic site [53], stabilizing the transition state of the substrate during RNA cap modification [54]. This electric quadrupole may be a potential target for antiviral therapy. Electric charge-based catalytic residues of the RNA polymerase Nsp12 have been identified in SARS-CoV-2: two negative aspartic acid residues, Asp618 and Asp760. Together with these two aspartic acid residues, Asp623 and Asp761 are involved in the recognition of NTP triphosphate and divalent cations, respectively [55]. Moreover, the D760A mutant in SARS-CoV Nsp12, which loses its negative charge, cannot synthesize RNA [56].

During lysosomal virus release, SARS-CoV-2 ORF3a carries a negative charge, −16 [e], in the domain upstream of Tyr145 that interacts with the center of membrane caveolin between residues Asp82 and Arg101, which has a charge of +2 [e] (data from RCSB PDB: > 6XDC_1|Chains A, B|ORF3a protein|Severe acute respiratory syndrome coronavirus 2 (2697049) and RCSB PDB: >7SC0_1|Chains A–K|Caveolin-1|Homo sapiens (9606)). ORF3a mutations causing a charge change are very rare and result in the loss of positive charge [57].

It seems that the positive charge of the spike protein of SARS-CoV-2 has an impact on treatment prognosis (3.4). When comparing the reports of Public Health England in June and September 2021 [31,32], a decrease in the percentage of fatal cases caused by the main SARS-CoV-2 variants was observed. This outcome was probably due to an increase in the size of the subpopulation younger than 50 years old infected by the virus, as they exhibited a higher survival rate than older patients. On the other hand, when comparing the September 2021 data for people 50+ years old with the total cases reported in June 2021, this decrease in fatal cases was not observed; rather, an increasing trend in the number of fatal cases was found along with an increase in the positive electric charge in crucial regions (RBD and S1/S2) of spike protein S, as reported in our earlier paper [39]. Therefore, the positive electric charge in crucial regions (RBD and S1/S2) of spike protein S may be important to the survival rate of the infected subpopulation that was 50+ years old. The comparison of September 2021 data for the 50+ cohort with the total case data reported in June 2021 is presented in Figure 6a. To the present, almost all of the virus variants exhibit mutations in the receptor binding motif (RBM), increasing local electric charge, Figure 6b. The most characteristic mutation is E484K (+2[e]). The most positive total change in RBM (+5 [e]) is observed for the Omicron variant. This probably increases the rate of virus-cell entering and the rate of its replication, both being evolutionary beneficial.

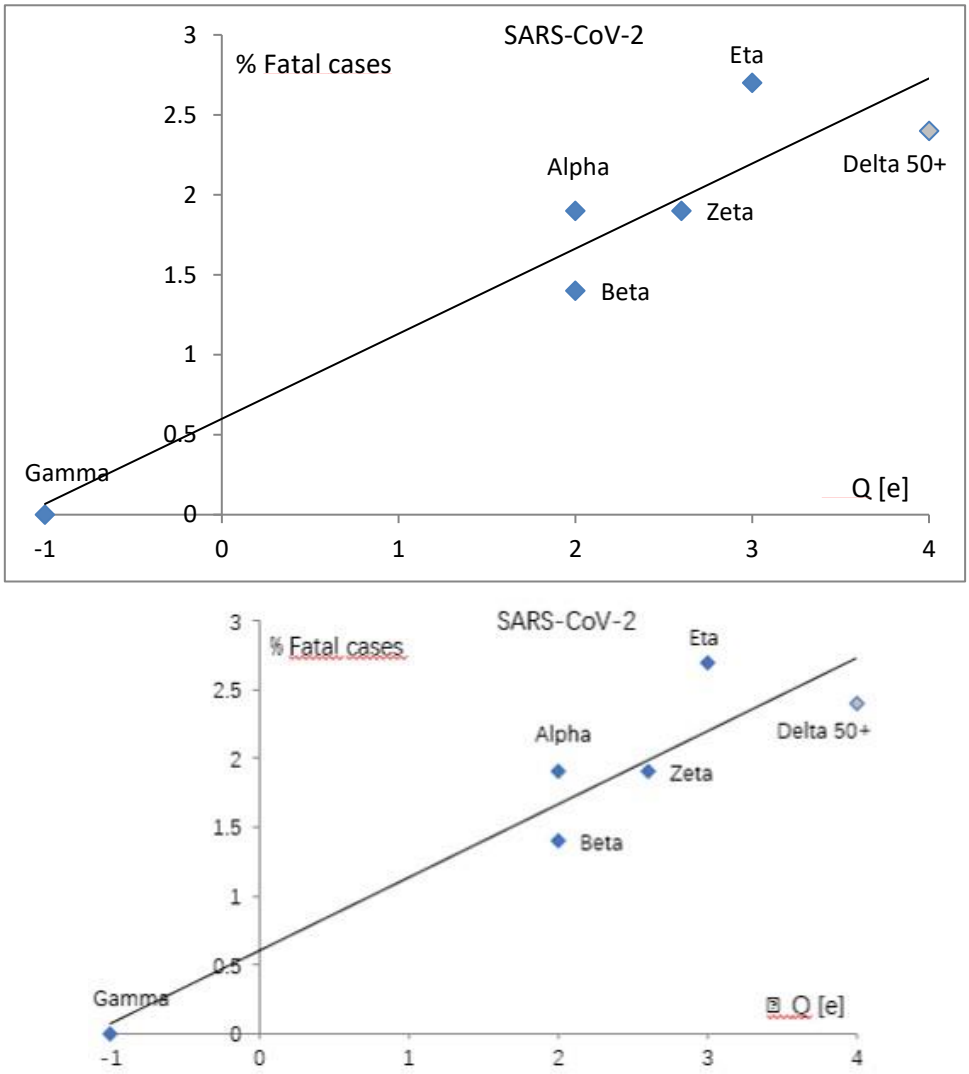

Figure 6a. The COVID-19 percentage of fatal cases versus the net charge change in the RBD and S1/S2 cleavage regions of spike protein S, according to Public Health England (September 2021) [31,32]. The arithmetic calculations of charge are based on the amino acids D, E, K, and R under physiological conditions. For simplicity, the value of an aa charge +/-1 [e] was assumed, and the charge of histidine was neglected. The reference "wild-type'" virus B.1 was used (with no D614G mutation or other spike protein changes) to calculate the change ΔQ. In the case of the WHO-labeled variants Alpha and Zeta, the mean change in the charge was calculated for 2 and 5 lineages, respectively. Only well-documented variants first detected in the UK, South Africa, Japan, and Brazil are presented. For the Delta variant of SARS-CoV-2, only data for the 50+-year age group were analyzed. Blue diamond markers indicate data from a previous paper [39]. The trend line y = 0,5322x + 0,5991, and R^2 = 0,8904.

Figure 6b. Multiple sequence alignment (MSA) of the receptor binding motif (RBM) in SARS-CoV-2 variants (May 2024), positions 438–508. Mutations are marked in red. The right column contains the mutation description and final electric charge change ([e]). The data for non-mutated "wild-type" strain were taken from Table 2, ref. a. Other data for mutated variants were taken from the Stanford University Coronavirus Antiviral & Resistance Database (https://covdb.stanford.edu/variants/alpha/). The following variants (lineages) are: Alpha (B.1.1.7), Beta (B.1.351), Gamma (P.1), Delta (B1.617.2), Epsilon (B1.427, B.1.429), Zeta (P.2), Eta (B.1.525), Theta (P.3), Iota (B.1.526), Kappa (B.1.617.1), Lambda (C.37), Mu (B1.621), and Omicron (B.1.1.529). A red font color means a positive charge increase, green means a neutral change, and black means that there is no mutation. Note that RBM is a smaller part of RBD.

It is widely accepted that virus charge and charge distribution determine drug targeting [58]. Additionally, immunity may depend on virus charge, as the outer leaflet of SARS-CoV-2 virions contains significant quantities of PS, favoring infection [59]. Notably, when the leaflet of a cell membrane facing the extracellular matrix contains the negatively charged lipid phosphatidylserine, macrophages sense that apoptosis has occurred and digest the cell [60]. This feature of macrophages may be applied to the treatment of COVID-19, but one problem may confound this possibility.

It was recently reported [61] that macrophages expressing CD169, a myeloid cell-specific I-type lectin, were highly permissive to viral entry and the initiation of viral replication, but completion of the viral life cycle was blocked, which prevented the production of new infectious virus particles. Surprisingly, this reduction in the entry and initiation of viral replication and expression of abortive viral transcripts in CD169+ macrophages was sufficient to activate host surveillance mechanisms (innate immune response) and induce proinflammatory cytokine expression (TNFα, IL-6, and IL-1β). A lectin-facilitated ACE2-independent SARS-CoV-2 fusion protein was found to enter macrophages, which may have been related to the electrostatic interaction of the spike RBD and the negatively charged (−4.2 [e], as determined with protein calculator v3.4) 20–136 aa domain of CD169 (Q9BZZ2 ·SN_HUMAN) or due to spike protein sialylation [62]. Protein S may also prevent interactions between macrophage phosphatidylserine receptors and SARS-CoV-2 membrane lipids.

Concerning the initial findings, we wondered how virus–receptor attachment could be prohibited (3.5). In Figure 7, we show that the overall charge of the spike protein in SARS-CoV-2 and its receptor ACE2 depended on the pH of the environment. In pH ranges < 5.5 and pH > 8.5, the charges of both the viral and host proteins carried the same sign, and repulsion should have been observed. Although the picture is not the same for folded proteins, we might expect that, at least in the case of surface amino acids, the charge estimation error for folded proteins is acceptable. Therefore, the results from protein charge estimates are promising and worthy of further consideration.

The products of the charges of RBD and ACE2 at different pH values are presented in Figure 8. In the range 6 < pH < 8, the charges were stable and negative. Below and above this range, however, the charge was greatly increased. This is why the stomach cavity (pH = 1.5–2.0), skin (pH = 4.7), vagina (pH = 3.8–5.0), and gallbladder (pH = 8.2) are not suitable sites for viral expansion. Calculations of the pH of sea salt aerosol particles [60] showed that the pH decreased with elevation above sea level, from 5.5 at sea level to 4.0 at 400 m above sea level.

Another reports, [63,64], indicated a reduction in the numbers of COVID-19 cases and deaths per capita in the Gulf and Pacific U.S. coastlines relative to inland counties by approximately 25%–30% ($P < 0.05$), which may confirm that in addition to the expected hypertonic salt-induced reduced infectivity, low pH and electrostatic effects result in lower infection rates. This possibility indicates potential opportunities for spa and inhaler treatments for the prevention and therapy of mild disease, as well as for rehabilitation. Some studies have reported that the mitigation of a hyperinflammatory state requires CD169 blockade or inhibition of proinflammatory cytokine expression by macrophages. For treatment following the former strategy, the lectin charge needs to be taken into account.

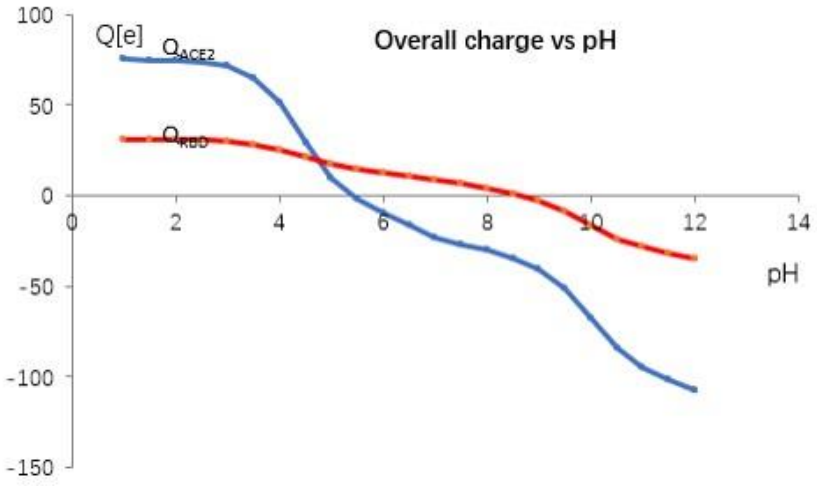

Figure 7. The overall charges of RBD and ACE2 (Q_{RBD} and Q_{ACE2}) as a function of the pH of the environment. Data are taken from **R**CSB PDB: >6M0J_1|Chain A|Angiotensin-converting enzyme 2|*Homo sapiens* (9606) and **R**CSB PDB: >6M0J_2|Chain B[auth E]|Spike protein S1|Severe acute respiratory syndrome coronavirus 2 (2697049). Protein calculator v3.4 was used for calculations (sourceforge.net). The values of Q_{RBD} and Q_{ACE2} were obtained by the amino acid exact charge analysis at different pH levels and summing them.

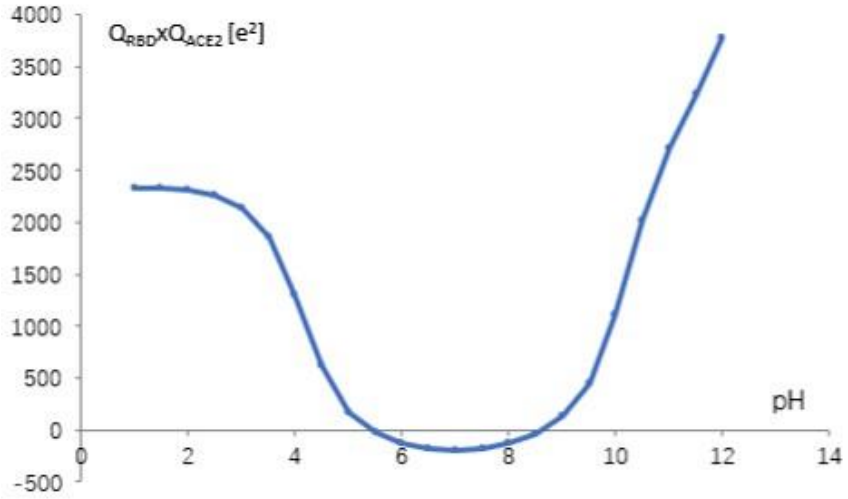

Figure 8. The charges product (the charge of RBD x the charge of ACE2) versus pH. The values of Q_{RBD} and Q_{ACE2} were obtained by the amino acid exact charge analysis at different pH levels with protein calculator v3.4 (sourceforge.net). They were presented before in Figure 7.

The difference in sign of the electric charge of the virus binding domain and host receptor, in SARS-CoV-2, Ebola, Dengue, influenza A, and RSV (Table 2) indicate the possible similar, electrostatic way of virus-cell approximation due to Coulombic attraction (3.6). Thus, the findings for SARS-CoV-2 may help in the prevention, or treatment, of other virial diseases. What is more, the importance of electrostatic interactions in the assembly and stability of viruses and their pH dependence is gaining more and more attention, and is confirmed by numerous experimental and theoretical studies regarding animal, plant, and artificial viruses [65–71].

As a result, one can expect that changing the charge relationship or pH between the virus and the cell surface can lead to suppression of the infection. According to our paper, neutralizing the virus charge outside the body should decrease its invasiveness, but it may not limit the spread of its replicants in the body. Then pH should be a key, but according to general knowledge, even a small change in natural pH in the organism may lead to undesirable consequences and therefore should be restricted only to the regime of the least-harm (short time, local small volume) conditions which are relatively poorly known. Of course, decontamination of medical equipment in high pH (8–9) may be freely considered.

Furthermore, in terms of disease transmission, the knowledge of the landscape (sign and position) of viral electric charges creates the possibility of finding practical solutions for effective electrostatic capture of viruses entering the body through different portals. Among others, it can be implemented in facial masks and respirators [72] containing electret fibers [73], ionizers producing neutralizing counterions [74,75], and electrostatic sprayers and foggers for the application of charged disinfectants [76]. Alternatively, the docking of short charged peptides to block RBD was proposed in [52].

What is more, the ACE2 receptor is not the only highly negatively charged component of the cell surface acting with the positively charged RBD in the S protein of SARS-CoV-2. The accompanying ACE2 heparan sulfate [77] interacts with the RBD as a cofactor facilitating its

opening. It may additionally increase the electrostatic attraction. Despite the virus charge, the role of electric parameters of the host cells, e.g., electrostatic surface potential [74], can be important. These factors should be considered in future theoretical investigations.

In our paper, the key role of electric charge and the interactions of electrically charged components involved in different aspects of virus infection are presented. These universal properties of viral infection may be very important elements, especially in the initial, replication, release, and immunization phases, so they should be carefully investigated in future research. Although the influence of the electric field on the cell's mechanical stability [78] is well-known, very little is known about how viruses use the electric charge to overcome the cell. Even though very simplified mathematical models of electrostatic interactions were presented, which do not take into account the real microscopic distribution of charges and their kinetics, which makes the brute-force simulation impossible and limits the analysis to the estimating method. We hope that this work reduces, to some extent, the level of our ignorance. It is still an open question if Coulomb electrostatics is a common way of virus-receptor interaction. For other viruses and more neutral electrostatic conditions, it may compete with van der Waals interactions. Also, the role of a charge at virus internalization through special structures, e.g., infected cell junction in direct cell-to-cell contact, which is known as the "virological synapse", should be examined [79]. Moreover, for docking at distances smaller than 0.5 nm, we may not meet the far distance limit and also observe the input of multipolar and chemical interactions, which may be important in contact inhibitor designing.

5. Conclusions

The presented results showed that the spatial distribution of electric charge may manifest itself in different areas during virus infection. Using SARS-CoV-2 as an example, it was shown that the local distribution of a charge may be more important than the overall charge, which is usually screened by counterions during virus infection. In this way, the local electric charge can determine virus–receptor attachment at the initial phase of infection and during the induction of the proinflammatory response. That means that electrostatic attraction may overcome the range of the hydrogen and van der Waals bonding. Additionally, the interactions of electrically charged nonstructural components, such as those described for catalytic processes, are important elements of human virus infection, and they are worth exploring to find new modes of protection against viral infection. The effective blocking of virus transmission based on the knowledge of the electrical charges associated with it seems to be a promising prospect.

Use of AI tools declaration

The authors declare that they have not used artificial intelligence (AI) tools in the creation of this article.

Conflict of interest

The authors declare that there are no conflicts of interest.

Author contributions

PH Pawłowski: Conceived and designed the theoretical models, analyzed data, and drafted the manuscript. P Zielenkiewicz: Critical feedback, data analysis, and revised the manuscript.

References

1. Viral Infections, *Physiopedia*, 2022. Available from: http:///index.php?title=Viral_Infections&oldid=290753
2. Betts MJ, Russell RB (2003) Amino acid properties and consequences of subsitutions, In: Barnes M.R., Gray I.C., *Bioinformatics for Geneticists*, Wiley, 289–316. https://doi.org/10.1002/0470867302.ch14
3. Lipfert J, Doniach S, Das R, et al. (2014) Understanding nucleic acid-ion interactions. *Annu Rev Biochem* 83: 813–841. https://doi.org/10.1146/annurev-biochem-060409-092720
4. Ma Y, Poole K, Goyette J, et al. (2017) Introducing membrane charge and membrane potential to T cell signaling. *Front Immunol* 8: 1513. https://doi.org/10.3389/fimmu.2017.01513
5. Zhao X, Ma X, Dupius JH, et al. (2022) Negatively charged phospholipids accelerate the membrane fusion activity of the plant-specific insert domain of an aspartic protease. *J Biol Chem* 298: 101430. https://doi.org/10.1016/j.jbc.2021.101430
6. Cruz-Chu ER, Malafeev A, Pajarskas T, et al. (2014) Structure and response to flow of the glycocalyx layer. *Biophys J* 106: 232–242. https://doi.org/10.1016/j.bpj.2013.09.060
7. Debye P, Hückel E (1923) The theory of electrolytes. I. Lowering of freezing point and related phenomena (PDF). *Physikalische Zeitschrift* 24: 185–206.
8. Michen B, Graule T (2010) Isoelectric points of viruses. *J Appl Microbiol* 109: 388–397. https://doi.org/10.1111/j.1365-2672.2010.04663.x
9. Heffron J, Mayer BK (2021) Virus isoelectric point estimation: theories and methods. *J Appl Environ Microb* 87: e02319–e02320. https://doi.org/10.1128/AEM.02319-20
10. Luisetto M, Tarro G, Edbey K, et al. (2021) Coronavirus COVID-19 surface properties: electrical charges status. *Int J Clin Microbiol Biochem Technol* 4: 016–027. https://doi.org/10.12688/f1000research.108667.2
11. Cavezzi A, Menicagli R, Troiani E, et al. (2022) COVID-19, cation dysmetabolism, sialic acid, CD147, ACE2, viroporins, hepcidin and ferroptosis: a possible unifying hypothesis. *F1000Res* 11: 102. https://doi.org/ 10.12688/f1000research.108667.2
12. Northwestern University, "Research exposes new vulnerability for SARS-CoV-2: Electrostatic interactions enhance the spike protein's bond to host cells." ScienceDaily, 2020, Available from: https://www.sciencedaily.com/releases/2020/08/200811120227.htm
13. Leung WWF, Sun Q (2020) Electrostatic charged nanofiber filter for filtering airborne novel coronavirus (COVID-19) and nano-aerosols. *Sep Purif Technol* 250: 116886. https://doi.org/10.1016/j.seppur.2020.116886
14. Corrêa Giron C, Laaksonen A, Barroso da Silva FL (2020) On the interactions of the receptor-binding domain of SARS-CoV-1 and SARS-CoV-2 spike proteins with monoclonal antibodies and the receptor ACE2. *Virus Res* 285: 198021. https://doi.org/10.1016/j.virusres.2020.198021

15. Chavda VP, Bezbaruah R, Deka K, et al. (2022) The delta and omicron variants of SARS-CoV-2: What we know so far. *Vaccines* 10: 1926. https://doi.org/10.3390/vaccines10111926
16. Carabelli AM, Peacock TP, Thorne LG, et al. (2023) SARS-CoV-2 variant biology: immune escape, transmission and fitness. *Nat Rev Microbiol* 21: 162–177. https://doi.org/10.1038/s41579-022-00841-7
17 Chavda VP, Patel AB, Vaghasiya DD (2022) SARS-CoV-2 variants and vulnerability at the global level. *J Med Virol* 94: 2986–3005. https://doi.org/10.1002/jmv.27717
18. Chavda VP, Ghali ENHK, Yallapu MM, et al. (2022) Therapeutics to tackle Omicron outbreak. *Immunotherapy* 14: 833–838. https://doi.org/10.2217/imt-2022-0064
19. Chavda VP, Vuppu S, Mishra T, et al. (2022) Recent review of COVID-19 management: diagnosis, treatment and vaccination. *Pharmacol Rep* 74: 1120–1148. https://doi.org/10.1007/s43440-022-00425-5
20. Polatoğlu I, Oncu-Oner T, Dalman I, et al. (2023) COVID-19 in early 2023: Structure, replication mechanism, variants of SARS-CoV-2, diagnostic tests, and vaccine & drug development studies. *MedComm* 4: e228. https://doi.org/10.1002/mco2.228
21. Basu D, Chavda VP, Mehta AA (2022) Therapeutics for COVID-19 and post COVID-19 complications: an update. *Curr Res Pharmacol Drug Discov* 3: 100086. https://doi.org/10.1016/j.crphar.2022.100086
22. Lancet T (2023) The COVID-19 pandemic in 2023: far from over. *Lancet* 401: 79. https://doi.org/10.1016/s0140-6736(23)00050-8
23. Arbeitman CR, Rojas P, Ojeda-May P, et al. (2021) The SARS-CoV-2 spike protein is vulnerable to moderate electric fields. *Nat Commun* 12 5407. https://doi.org/10.1038/s41467-021-25478-7
24. Božič A, Podgornik R (2024) Changes in total charge on spike protein of SARS-CoV-2 in emerging lineages. *Bioinformatics Adv* 4: vbae053. https://doi.org/10.1093/bioadv/vbae053
25 Javidpour L, Božič A, Naji A, et al. (2020) Electrostatic interaction between SARS-CoV-2 virus and charged electret fibre. *Soft Matter* 17: 4296–4303. https://doi.org/10.1039/D1SM00232E
26. Zhang Z, Zhang J, Wang J (2022) Surface charge changes in spike RBD mutations of SARS-CoV-2 and its variant strains alter the virus evasiveness *via* HSPGs: a review and mechanistic hypothesis. *Front Public Health* 10: 952916. https://doi.org/10.3389/fpubh.2022.952916
27. Bar-On YM, Flamholz A, Phillips R, et al. (2020) SARS-CoV-2 (COVID-19) by the numbers. *elife* 9: e57309. https://doi.org/10.7554/eLife.57309
28. Berman HM, Westbrook J, Feng Z, et al. (2000) The protein data bank. *Nucleic Acids Res* 28: 235–242. https://doi.org/10.1093/nar/28.1.235
29. Sayers EW, Bolton EE, Brister JR, et al. (2022) Database resources of the national center for biotechnology information. *Nucleic Acids Res* 50: D20–D26. https://doi.org/10.1093/nar/gkab1112
30. Jiao LG, Zan LR, Zhu L, et al. (2019) Accurate computation of screened Coulomb potential integrals in numerical Hartree–Fock programs. *Comput Phys Commun* 244: 217–227. https://doi.org/10.1016/j.cpc.2019.06.001

31. SARS-CoV-2 variants of concern and variants under investigation in England Technical briefing 15, Public Health England, 2021. Available from: https://assets.publishing.service.gov.uk/government/uploads/system/uploads/attachment_data/file/993879/Variants_of_Concern_VOC_Technical_Briefing_15.pdf.
32. SARS-CoV-2 variants of concern and variants under investigation in England Technical briefing 23. Public Health England, PHE2, 2021. Available from: https://assets.publishing.service.gov.uk/government/uploads/system/uploads/attachment_data/file/1018547/Technical_Briefing_23_21_09_16.pdf.
33. Adamczyk Z, Batys P, Barbasz J (2021) SARS-CoV-2 virion physicochemical characteristics pertinent to abiotic substrate attachment. *Curr Opin Colloid Interface Sci* 55: 101466. https://doi.org/10.1016/j.cocis.2021.101466
34. Berger O, Edholm O, Jähnig F (1997) Molecular dynamics simulations of a fluid bilayer of dipalmitoylphosphatidylcholine at full hydration, constant pressure, and constant temperature. *Biophys J* 72 : 2002–2013. https://doi.org/10.1016/S0006-3495(97)78845-3
35. Krebs F, Scheller C, Grove-Heike K (2021) Isoelectric point determination by imaged CIEF of commercially available SARS-CoV-2 proteins and the hACE2 receptor. *Electrophoresis* 42: 687–692. https://doi.org/10.1002/elps.202100015
36. Pawłowski PH (2021) SARS-CoV-2 variant Omicron (B.1.1.529) is in a rising trend of mutations increasing the positive electric charge in crucial regions of the spike protein S. *Acta Biochim Pol* 69: 263–264. https://doi.org/10.18388/abp.2020_6072
37. Cotten M, Phan M (2022) Evolution to increased positive charge on the viral spike protein may be part of the adaptation of SARS-CoV-2 to human transmission. *iScience* 26: 106230. https://doi.org/10.1016/j.isci.2023.106230
38. Lu Y, Zhao T, Lu M, et al. (2021) The analyses of high infectivity mechanism of SARS-CoV-2 and its variants. *COVID* 1: 666–673. https://doi.org/10.3390/covid1040054
39. Pawłowski PH (2021) Additional positive electric residues in the crucial spike glycoprotein S regions of the new SARS-CoV-2 variants. *Infect Drug Resist* 14: 5099–5105. https://doi.org/10.2147/IDR.S342068
40. Bromage E, The risks-know them-avoid them, 2020. Available from: https://www.erinbromage.com/post/the-risks-know-them-avoid-them.
41. Islam MA, Ford Versypt AN (2022) Mathematical modeling of impacts of patient differences on COVID-19 lung fibrosis outcomes. bioRxiv [Preprint] https://doi.org/10.1101/2022.11.06.515367
42. Coulomb CA (1785) Premier mémoire sur l'électricité et le magnétisme" [First dissertation on electricity and magnetism]. Histoire de l'Académie Royale des Sciences [History of the Royal Academy of Sciences] (in French), 569–577. https://www.academie-sciences.fr/pdf/dossiers/Coulomb/Coulomb_pdf/Mem1785_p569.pdf
43. Kobayashi Y, Suzuki Y (2012) Compensatory evolution of net-charge in influenza A virus hemagglutinin. *PLoS One* 7: e40422. https://doi.org/10.1371/journal.pone.0040422
44. Xia S, Liu M, Wang C, et al. (2020) Inhibition of SARS-CoV-2 (previously 2019-nCoV) infection by a highly potent pan-coronavirus fusion inhibitor targeting its spike protein that harbors a high capacity to mediate membrane fusion. *Cell Res* 30: 343–355. https://doi.org/10.1038/s41422-020-0305-x

45. Brunton B, Rogers K, Phillips EK, et al. (2019) TIM-1 serves as a receptor for Ebola virus in vivo, enhancing viremia and pathogenesis. *PLoS Negl Trop Dis* 13: e0006983. https://doi.org/10.1371/journal.pntd.0006983
46. Fahimi H, Allahyari H, Hassan ZM, et al. (2014) Dengue virus type-3 envelope protein domain III; expression and immunogenicity. *Iran J Basic Med Sci* 11: 836–843.
47. Saad-Roy CM, Arinaminpathy N, Wingreen NS, et al. (2020) Implications of localized charge for human influenza A H1N1 hemagglutinin evolution: insights from deep mutational scans. *PLoS Comput Biol* 16: e1007892. https://doi.org/10.1371/journal.pcbi.1007892
48. Feng Z, Xu L, Xie Z (2022) Receptors for respiratory syncytial virus infection and host factors regulating the life cycle of respiratory syncytial virus. *Front Cell Infect Microbiol* 12: 858629. https://doi.org/10.3389/fcimb.2022.858629
49. Petrache HI, Tristram-Nagle S, Gawrisch K, et al. (2004) Structure and fluctuations of charged phosphatidylserine bilayers in the absence of salt. *Biophys J* 86: 1574–1586. https://doi.org/10.1016/S0006-3495(04)74225-3
50. Varki A, Schauer R (2009) Sialic Acids. In: Varki A., Cummings R.D., Esko J.D., et al. *Essentials of Glycobiology*, 2 Eds., Cold Spring Harbor (NY): Cold Spring Harbor Laboratory Press.
51. Lupala CS, Lil X, Lei J, et al. (2021) Computational simulations reveal the binding dynamics between human ACE2 and the receptor binding domain of SARS-CoV-2 spike protein. *Quant Biol* 9: 61–72. https://doi.org/10.15302/J-QB-020-0231
52. Pawłowski PH (2021) Charged amino acids may promote coronavirus SARS-CoV-2 fusion with the host cell. *AIMS Biophys* 8: 111–121. https://doi.org/10.3934/biophy.2021008
53. Romano M, Ruggiero A, Squeglia F,et al. (2020) A structural view of SARS-CoV-2 RNA replication machinery: RNA synthesis, proofreading and final capping. *Cells* 9: 1267. https://doi.org/10.3390/cells9051267
54. Silva JRA, Urban J, Araújo E, et al. (2022) Exploring the catalytic mechanism of the RNA cap modification by nsp16-nsp10 complex of SARS-CoV-2 through a QM/MM approach. *Int J Mol Sci* 23: 300. https://doi.org/10.3390/ijms23010300
55. Kirchdoerfer RN, Ward AB (2019) Structure of the SARS-CoV nsp12 polymerase bound to nsp7 and nsp8 co-factors. *Nat Commun* 10: 2342. https://doi.org/10.1038/s41467-019-10280-3
56. Subissi L, Posthuma CC, Collet A, et al. (2014) One severe acute respiratory syndrome coronavirus protein complex integrates processive RNA polymerase and exonuclease activities. *Proc Natl Acad Sc USA* 111: E3900–E3909. https://doi.org/10.1073/pnas.1323705111
57. Bianchi M, Borsetti A, Ciccozzi M, et al. (2021) SARS-Cov-2 ORF3a: mutability and function. *Int J Biol Macromol* 15: 820–826. https://doi.org/10.1016/j.ijbiomac.2020.12.142
58. Scheller C, Krebs F, Minkner R, et al. (2020) Physicochemical properties of SARS-CoV-2 for drug targeting, virus inactivation and attenuation, vaccine formulation and quality control. *Electrophoresis* 41: 1137–1151. https://doi.org/10.1002/elps.202000121
59. Bohan D, Ert HV, Ruggio N, et al. (2021) Phosphatidylserine receptors enhance SARS-CoV-2 infection. *PLoS Pathog* 17: e1009743. https://doi.org/10.1371/journal.ppat.1009743
60. Alberts B, Johnson A, Lewis J, et al. (2002) *Molecular Biology of the Cell*, 4 Eds. New York: Garland Science.

61. Jalloh S, Olejnik J, Berrigan J, et al. (2022) CD169-mediated restrictive SARS-CoV-2 infection of macrophages induces pro-inflammatory responses. *PLoS pathogens* 18: e1010479. https://doi.org/10.1371/journal.ppat.1010479
62. Watanabe Y, Allen JD, Wrapp D, et al. (2020) Site-specific glycan analysis of the SARS-CoV-2 spike. *Science* 369: 330–333. https://doi.org/10.1126/science.abb9983
63. von Glasow R, Sander R (2001) Variation of sea salt aerosol pH with relative humidity. *Geophys Res Lett* 28: 247–250. https://doi.org/10.1029/2000GL012387
64. Field RD, Moelis N, Salzmann J, et al. (2021) Inhaled water and salt suppress respiratory droplet generation and COVID-19 incidence and death on US coastlines. *Mol Front J* 5.01n02: 17–29. https://doi.org/10.1142/S2529732521400058
65. Duran-Meza AL, Villagrana-Escareño MV, Ruiz-García J, et al. (2021) Controlling the surface charge of simple viruses. *PLoS One* 16: e0255820. https://doi.org/10.1371/journal.pone.0255820
66. Vega-Acosta JR, Cadena-Nava RD, Gelbart WM, et al. (2014) Electrophoretic mobilities of a viral capsid, its capsid protein, and their relation to viral assembly. *J Phys Chem B* 118: 1984–1989. https://doi.org/10.1021/jp407379t
67. Bockstahler LE, Kaesberg P (1962) The molecular weight and other biophysical properties of bromegrass mosaic virus. *Biophys J* 2: 1962. https://doi.org/10.1016/s0006-3495(62)86836-2
68. Johnson MW, Wagner GW, Bancroft JB (1973) A titrimetric and electrophoretic study of cowpea chlorotic mottle virus and its protein. *J Gen Virol* 19: 263–273. https://doi.org/10.1099/0022-1317-19-2-263
69. van der Schoot P, Bruinsma R (2005) Electrostatics and the assembly of an RNA virus. *Phys Rev E* 71: 061928. https://doi.org/10.1103/PhysRevE.71.061928
70. Belyi VA, Muthukumar M (2006) Electrostatic origin of the genome packing in viruses. *Proc Natl Acad Sci* 103: 17174–17178. https://doi.org/10.1073/pnas.0608311103
71. Hagan MF (2009) A theory for viral capsid assembly around electrostatic cores. *J Chem Phys* 130: 114902. https://doi.org/10.1063/1.3086041
72. Lorenzo-Leal AC, Vimalanathan S, Bach H (2022) Adherence of SARS-CoV-2 delta variant to a surgical mask and N95 respirators. *Future Sci OA* 8: FSO808. https://doi.org/10.2144/fsoa-2022-0025
73. Javidpour L, Božič A, Najili A, et al. (2021) Electrostatic interaction between SARS-CoV-2 virus and charged electret fibre. *Soft Matter* 17: 4296–4203. https://doi.org/10.1039/D1SM00232E
74. Ren C, Haghighat F, Feng Z, et al. (2023) Impact of ionizers on prevention of airborne infection in classroom. *Build Simul* 16: 749–764. https://doi.org/10.1007/s12273-022-0959-z
75. Fantini J, Azzaz F, Chahinian H, et al. (2023) Electrostatic surface potential as a key parameter in virus transmission and evolution: How to manage future virus pandemics in the post-COVID-19 era. *Viruses* 15: 284. https://doi.org/10.3390/v15020284
76. Wood JP, Magnuson M, Touati A, et al. (2021) Hook Evaluation of electrostatic sprayers and foggers for the application of disinfectants in the era of SARS-CoV-2. *PLoS One* 16: e0257434. https://doi.org/10.1371/journal.pone.0257434
77. Kalra RS, Kandimalla R (2021) Engaging the spikes: heparan sulfate facilitates SARS-CoV-2 spike protein binding to ACE2 and potentiates viral infection. *Sig Transduct Target Ther* 6: 39. https://doi.org/10.1038/s41392-021-00470-1

78. Pawłowski P, Szutowicz I, Marszałek P, et al. (1993) Bioelectrorheological model of the cell. 5. Electrodestruction of cellular membrane in alternating electric field. *Biophys J* 65: 541–549. https://doi.org/10.1016/S0006-3495(93)81056-7
79. Igakura T, Stinchcombe JC, Goon PK, et al. (2003) Spread of HTLV-I between lymphocytes by virus-induced polarization of the cytoskeleton. *Science* 299: 1713–1716. https://doi.org/10.1126/science.1080115

AIMS Press